Research Square

Preprints are preliminary reports that have not undergone peer review.
They should not be considered conclusive, used to inform clinical practice,
or referenced by the media as validated information.

Characterising the solar-coronal electron density with BepiColombo multi-frequency range measurements

Irene Doria

irene.doria@uniroma1.it

Sapienza University of Rome: Universita degli Studi di Roma La Sapienza https://orcid.org/0000-0001-7435-466X

Paolo Cappuccio

SSC Space for ESA/ESAC

Luciano Iess

Sapienza University of Rome: Universita degli Studi di Roma La Sapienza

Research Article

Keywords: BepiColombo, solar plasma, radio science, electron density

Posted Date: November 10th, 2026

DOI: https://doi.org/10.21203/rs.3.rs-11280210/v1

License: This work is licensed under a Creative Commons Attribution 4.0 International License.
Read Full License

Characterising the solar-coronal electron density with BepiColombo multi-frequency range measurements

Irene Doria[1], irene.doria@uniroma1.it

Paolo Cappuccio[2], paolo.cappuccio@ext.esa.int

Luciano Iess[1], luciano.iess@uniroma1.it

Affiliations

1. Sapienza University of Rome, Department of Mechanical and Aerospace Engineering (DIMA), Rome, Italy
2. SSC Space for ESA/ESAC, Villafranca Del Castillo, Spain

Corresponding author

Irene Doria, irene.doria@uniroma1.it

Abstract

The propagation of spacecraft radio signals through the solar corona is affected by dispersive delays induced by free electrons in the plasma, particularly during close solar approaches or superior solar conjunctions, when the line of sight passes at small heliocentric distances. Models of the electron density and its variations are important both for predicting measurement noise in radiometric measurements and for assessing telecommunication channels of deep space missions across solar conjunctions. In this work, we use radiometric data of the ESA probe BepiColombo to assess and refine empirical descriptions of the average electron-density distribution in the solar corona. During superior solar conjunctions, the spacecraft radio link probes the inner corona, where solar plasma represents by far the dominant contribution to the path delay. The mission's multi-frequency X- and Ka-band radio system allows a full separation of the plasma contribution from the non-dispersive component of the signal, enabling the exploitation of calibrated range observables for investigations of the solar corona. We analyse data acquired during five BepiColombo superior solar conjunction experiments in the rising phase of solar cycle 25, focusing on range measurements as a direct probe

of the plasma-induced path delay. Unlike Doppler observables, which are sensitive to temporal variations in the integrated electron content along the propagation path, multi-frequency range measurements provide access to the absolute total electron content. We use these measurements to constrain radial electron-density profiles at heliocentric distances larger than approximately four solar radii. The results show that, for the BepiColombo data set considered here, a single-power-law radial model provides a robust representation of the average coronal electron-density behaviour, while the additional degree of freedom introduced by a two-terms model is not significantly constrained by the observations. However, the measurements show significant deviations from all tested models due to the non-stationarity of the solar activity.

Keywords

BepiColombo, solar plasma, radio science, electron density

1 Introduction

The solar corona is a dispersive propagation medium for spacecraft radio signals: its

45 free electrons introduce frequency-dependent delays that become particularly significant
46 when the radio path passes close to the Sun. This same effect makes radio signals a
47 powerful mean to probe the coronal plasma and, in particular, its electron density,
48 which has been studied using a variety of observational techniques. One such technique
49 is the Very Long Baseline Interferometry (VLBI), which uses distant natural radio
50 sources. When the line of sight between the radio source and Earth passes close to the
51 Sun, the radio waves traverse the solar corona before being detected by two or more
52 terrestrial antennas, thereby enabling detailed investigations of coronal properties
53 (Spangler et al., 2002; Soja et al., 2014).
54 Another technique exploits the effect of the solar plasma on spacecraft radio links.
55 Several missions have used solar conjunction (see Figure 1) to study the solar corona.
56 For example, the Viking mission used the radio links of its telecommunication and
57 tracking system (Johnston et al., 1977) and conducted solar corona experiments during
58 solar conjunctions of Mars. These data have been used in many works to derive electron
59 density models for the solar plasma (Tyler et al., 1977; Muhleman and Anderson, 1981,
60 Berman and Wackley, 1977). Radio links have also been used for solar plasma studies

61 by Mariner 6 and Mariner 7 (Muhleman et al., 1977), and Ulysses (Bird et al., 1994;
62 1996) among others, and more recently by Cassini (Morabito, 2007) and BepiColombo
63 (Cappuccio et al., 2024).
64 While Viking was equipped with an S- and X-band dual-frequency link, Cassini and
65 BepiColombo carry X- and Ka-band transponders (Kliore et al., 2004; Iess et al., 2021),
66 which enable a nearly complete cancellation of plasma noise and thus more accurate
67 measurements.
68 BepiColombo, a joint mission of the European Space Agency (ESA) and the Japan
69 Aerospace Exploration Agency (JAXA), was launched on 20 October 2018 from the
70 Kourou spaceport in French Guyana. The spacecraft is currently on its cruise phase to
71 Mercury, with arrival at the planet in November 2026 (Benkhoff et al., 2021).
72 The BepiColombo spacecraft carries a suite of sixteen experiments designed to
73 characterise Mercury, and among them there is the Mercury Orbiter Radio-science
74 Experiment (MORE) (Iess et al., 2021). The primary observables of MORE are range
75 and Doppler measurements, obtained through a multi-frequency radio link with two
76 uplink and three downlink carriers in X- and Ka-band. In this work, we exploit superior

77 solar conjunctions, a geometrical configuration in which the Sun lies between the Earth
78 and the spacecraft (see Figure 1). During these events the radio signal traverses regions
79 close to the Sun, with impact parameters (denoted b in Figure 1) as small as a few solar
80 radii. As a result, the radiometric observables are affected by increased dispersive noise.
81 The contribution of the coronal plasma can be isolated through accurate calibration
82 (Bertotti et al., 1993) and can be used to characterise the inner solar corona.
83 In this paper we use the data set acquired by BepiColombo during five solar conjunction
84 experiments, focusing on range observables to study electron density models. This
85 extensive data set allows the electron-density distribution to be sampled across different
86 phases of the solar cycle and over a range of heliocentric distances. Moreover, it is the
87 first time that range data are available separately on the uplink and downlink legs, with
88 an improved accuracy with respect to the past missions.
89 Section 2 presents the BepiColombo radio-tracking system and the plasma calibration
90 method, followed by a brief description of the solar conjunction experiments. Section 3
91 summarises the main electron density models available in the literature. Section 4
92 describes the measurement principle and the methodology used to retrieve the total

93 electron content from the range observables. Section 5 reports the results of the electron
94 density model obtained with the BepiColombo data. Finally, Section 6 discusses and
95 summarises the results of this analysis.
96
97 **Figure 1** Scheme representing the configuration of Sun (S), Earth (E) and probe (P)
98 during the superior solar conjunction.
99
100 ## 2 Observations
101 ### 2.1 Radio-tracking system
102 The BepiColombo radio system consists of a multi-frequency link configuration, where
103 three links can be simultaneously established (with two uplink and three downlink
104 carriers).
105 This configuration is possible thanks to the Ka-band transponder (KaT) and the Deep
106 Space Transponder (DST): the KaT allows to establish the coherent links in Ka-band
107 between ground station and spacecraft (the uplink at 34.4 GHz and the downlink at 32.1
108 GHz), while the DST receives the X-band uplink carrier (at 7.2 GHz) and retransmits

109 the two X- and Ka-band downlinks, at 8.4 GHz and 32.0 GHz respectively (Iess et al.,
110 2021). The Ka-band link established by the KaT will be the primary link for the radio
111 science experiment MORE, while the X- and Ka-band links established by the DST are
112 used by MORE for the elimination of the plasma noise. The configuration scheme is
113 reported in Figure 2.
114 A signal with a very stable frequency is transmitted from the ground station to the
115 spacecraft; the onboard transponder receives the signal and retransmits it coherently to
116 ground. To avoid interferences between the uplink and downlink signals, the latter is
117 frequency-shifted by the turn-around-ratio, α. Range data are obtained by measuring
118 the time delay between transmission and reception of a known modulation of the
119 carrier; in particular, MORE uses the PN (pseudo-noise) ranging system ("Pseudo-
120 Noise ranging system", Blue Book, 2022).
121
122 **Figure 2** Configuration scheme of the BepiColombo radio system. The Ka/Ka link
123 requires the KaT transponder on board, while the X/X and X/Ka links are established
124 thanks to the DST. TWTA stands for Traveling Wave Tube Amplifier and SSA stands

for Solid State Amplifier (see Iess et al., 2021).

The MORE data analysed in this work were collected with the ESTRACK DSA 3 ground antenna located in Malargüe, Argentina. DSA 3 is a beam-waveguide antenna equipped with X- and Ka-band transmitters and receivers (Iess et al., 2021); it fully supports multi-frequency links and is also equipped with a water vapour radiometer for wet tropospheric delay calibrations (Lasagni Manghi et al., 2023).

2.2 Plasma calibrations

The multi-frequency radio-link configuration enables the plasma contribution to be isolated because of its dispersive nature, namely because the plasma-induced delay depends on the signal frequency. At microwave frequencies, the refractive index of a plasma differs from unity by an amount proportional to the inverse square of the carrier frequency. Consequently, lower-frequency signals experience larger plasma-induced delays than higher-frequency signals.

The BepiColombo triple link configuration allows to nearly completely isolate the plasma noise from the data (Doria et al., 2025a). In fact, in this configuration three

observable quantities are considered, $y_{X/X}^{obs}$, $y_{X/Ka}^{obs}$ and $y_{Ka/Ka}^{obs}$, where y can represent the path delay variation or the relative frequency shift. Combining these measurements, it is possible to obtain three unknown quantities: the non-dispersive path delay variation or relative frequency shift y_{nd}, and the contributions from the uplink and downlink plasma at a reference frequency, y_{pl_up} and y_{pl_dn}.

It's then possible to write the following expressions (in the geometric optics limit) (Bertotti et al., 1993; Tortora et al., 2004):

$$
\begin{aligned}
y_{X/X}^{obs} &= y_{nd} + y_{pl_up} + \frac{1}{\alpha_{X/X}^2} y_{pl_dn} \\
y_{X/Ka}^{obs} &= y_{nd} + y_{pl_up} + \frac{1}{\alpha_{X/Ka}^2} y_{pl_dn} \qquad (1) \\
y_{Ka/Ka}^{obs} &= y_{nd} + \frac{1}{\beta^2} y_{pl_up} + \frac{1}{\beta^2 \alpha_{Ka/Ka}^2} y_{pl_dn}
\end{aligned}
$$

where:

- $\alpha_{X/X} = \frac{f_{X_D}}{f_{X_U}} = \frac{880}{749}$ is the turn-around ratio for the X/X link
- $\alpha_{X/Ka} = \frac{f_{K_D}}{f_{X_U}} = \frac{3344}{749}$ is the turn-around ratio for the X/Ka link
- $\alpha_{Ka/Ka} = \frac{f_{K_D}}{f_{K_U}} = \frac{3360}{3599}$ is the turn-around ratio for the Ka/Ka link
- $\beta = \frac{f_{K_U}}{f_{X_U}}$ is the ratio between the Ka- and X-band uplink frequencies

The transponding ratios are set by the International Telecommunications Union (ITU).

In the above equations the uplink and downlink plasma contributions y_{pl_up} and y_{pl_dn} are referred to an X-band uplink carrier. The subscripts D and U indicate the downlink and the uplink respectively. This set consists of three equations in three unknowns, so it can be solved to find the non-dispersive observable y_{nd} and the plasma contributions y_{pl_up} and y_{pl_dn}.

In this work the focus is on the analysis of the signal due to plasma, so the quantities y_{pl_up} and y_{pl_dn} from the calibrations of range data are the primary dataset of our analysis.

2.3 Solar conjunction experiment

In the configuration of a superior solar conjunction, the Sun, the spacecraft, and the Earth are nearly aligned, with the Sun located between the spacecraft and the Earth, as shown in Figure 1. This geometry is characterised using two angles: the Sun-Probe-Earth angle (SPE) and the Sun-Earth-Probe angle (SEP). The SEP angle is used for spacecraft located beyond Earth's orbit, whereas the SPE angle is used when the spacecraft is at heliocentric distances smaller than 1 AU. In both cases, superior solar conjunction is identified when the relevant angle approaches zero, indicating an almost

173 collinear Sun-spacecraft-Earth configuration.

174 In this study five solar conjunction experiments (SCE) are considered:

175 1. SCE1, which lasts from 10th to 24th March 2021

176 2. SCE2, which lasts from 29th January to 12th February 2022

177 3. SCE4, which lasts from 29th January to 12th February 2023

178 4. SCE5, which lasts from 26th June to 6th July 2023

179 5. SCE6, which lasts from 8th to 22nd December 2023

180 The geometries of these five experiments are reported in Figure 3, where the view from
181 the Earth in the plane orthogonal to the line of sight is shown and each dot represents a
182 ground tracking pass of the conjunction. Moreover, in order to validate the electron
183 density model also at longer distances, data from two cruise tests where the line of sight
184 was at high impact parameters are added to the analysis. The first cruise test goes from
185 7 to 11 September 2020, while the second test consists of 9 passes from 4 to 26
186 November 2020.

187

188 **Figure 3** Solar conjunctions' geometry represented in the plane orthogonal to the line of

189 sight as seen from the Earth. Each dot represents the middle of a tracking pass of the
190 conjunction, while the arrows indicate the direction towards which BepiColombo is
191 moving.
192
193 ## 3 Electron density models
194 Past studies analysed radiometric data to find a suitable electron density model for the
195 solar plasma and here we present the main ones that we have considered in our work.
196 The electron density models presented below are a derivation of the original Baumbach-
197 Allen model (Baumbach 1937; Allen 1947). The first model was proposed by
198 Baumbach (1937) and it's a function of the radial distance from the Sun:
199 $$N_e = 10^{14}\left(\frac{2.99}{r^{16}} + \frac{1.55}{r^{6}} + \frac{0.036}{r^{1.5}}\right) \quad e^{-}/m^3 \qquad (2)$$
200 This model was then adjusted by Allen (1947) who maintained only the first two terms.
201 Later models have been based on this structure and some of them have added an
202 additional term depending on the heliolatitude. Moreover, we have considered also a
203 single-term model.
204 ### 3.1 Tyler (1977)

205 The model proposed by Tyler (Tyler et al., 1977) is reported in the following equation:

206 $$N_e = \left[\left(\frac{2.99}{r^{16}} + \frac{1.55}{r^6}\right) \cdot 10^{14} + \frac{3.44}{r^2} \cdot 10^{11}\right]$$

207 $$\cdot \left(\cos^2(\theta) + \frac{1}{64}\sin^2(\theta)\right)^{\frac{1}{2}} \quad e^-/m^3 \quad (3)$$

208 where r is the distance from the centre of the Sun expressed in solar radii, θ is the

209 solar latitude and N_e is the electron number density. The first term can be considered

210 negligible for the impact parameters at stake, but the second term in r^{-6} cannot be

211 neglected in the BepiColombo case.

212 This model was derived from the data of Viking solar corona experiment during the

213 1976 Mars solar conjunction (at solar minimum). Data were obtained from 60 solar

214 radii to 0.3 solar radii (in X-band) and the radio paths sliced through a region of the

215 corona that included both equatorial and south polar latitudes of the Sun. It was

216 observed that the integrated plasma density near the south pole of the Sun generally

217 agreed with a model of the corona with a plasma density decreasing of a factor 1/8 from

218 the equator to the pole. The latitudinal term of Eq. (3) was derived from this

219 consideration.

220 **3.2 Berman and Wackley (1977)**

The model proposed by Berman and Wackley (Berman and Wackley, 1977; Bird 1982) also depends on radial distance and solar latitude:

$$N_e = \left[\frac{2.39 \cdot 10^{14}}{r^6} + \frac{1.67 \cdot 10^{12}}{r^{2.30}}\right] \cdot 10^{-\frac{0.9|\theta|}{90}} \quad e^-/m^3 \qquad (4)$$

The derivation exploited the data from Viking and Pioneer 10 and 11 solar conjunctions (1976) at solar minimum. Viking S-band Doppler root mean square (RMS) phase fluctuations and comparisons of Viking Doppler noise to Viking differenced S-X range measurements were used to compute the mean equatorial electron density model (dependence on r). Pioneer Doppler results were exploited to derive the heliographic latitude effect (dependence on θ).

3.3 Muhleman-Anderson (1981)

Another density profile was proposed by Muhleman and Anderson (Muhleman and Anderson, 1981):

$$N_e = \frac{1.32 \cdot 10^6}{r^{2.7}} \exp\left(-\frac{\theta^2}{(8°)^2}\right) + \frac{2.3 \cdot 10^5}{r^{2.04}} \quad e^-/cm^3 \qquad (5)$$

In order to derive this model, analyses of the two-frequency radio time-delay data from Viking were performed. A wide range of ray impact parameters was used: from 170 to 4.5 solar radii in the inbound phase of the 1976 conjunction and from 3.0 to 215 solar radii (1 AU) of the outbound phase. The solar latitudes were always below 6° except for

238 a few weeks around solar conjunction when the spacecraft appeared to pass the south
239 limb of the Sun. All pre-conjunction data had solar latitudes near 0°, but the post-
240 conjunction data probed the range from θ= 26° (south) back to nearly 0° in a few
241 weeks. Considering the small range of latitudes covered by the data set, the authors
242 assumed that the "sources" of the solar wind at the Sun were stochastic and Gaussian
243 distributed about the solar equator and that the resulting electron density variation with
244 latitude would be roughly Gaussian.

245 **3.4 Bird et al. (1994)**

246 Then, we have considered the single-term density model studied by Bird et al. (1994):

247 $$N_e = N_B \left(\frac{R_\odot}{r}\right)^{\alpha} e^-/m^3 \quad (6)$$

248 This model is based on the data from Ulysses solar conjunction in 1991 for a range of
249 solar distances from $4\ R_\odot$ to $40\ R_\odot$. During this conjunction only three points with
250 heliolatitude greater than 45° were recorded, thus the electron density model could be
251 reliably expressed by a single-power law. For the ingress phase of Ulysses, the
252 parameters in Eq. (6) have been estimated to be $\alpha = 2.54$ and $N_B = 3.61 \cdot 10^6\ cm^{-3}$,
253 while for the egress phase $\alpha = 2.42$ and $N_B = 2.26 \cdot 10^6\ cm^{-3}$.

3.5 Mercier-Hollweg (2019)

The most recent density profile model that we have analysed is from Mercier-Hollweg (Wexler et al., 2019):

$$N_e = \left(\frac{65}{r^{5.94}} + \frac{0.768}{(r-1)^{2.25}}\right) \times 10^{12} \quad e^-/m^3 \qquad (7)$$

This model is based on radio telescope observations of *MESSENGER* spacecraft in superior solar conjunction at solar minimum in 2009 and data of *HELIOS* 1 and 2 over 1975-6, again near a minimum of solar activity. This is a hybrid model derived in Wexler et al. (2019). It combines:

- Hollweg et al. (2010), that provided a number density model for a streamer along heliolatitude 28° over 2<R<30 solar radii with a formula:

$$N_e(r) = 7.68 \times 10^{11}(r-1)^{-2.25} \qquad (8)$$

- Average of 2008 and 2010 equatorial electron number density determinations from Mercier and Chambe (2015) fitted over 1.2-1.5 solar radii; this corresponds to an additional term applicable to low solar offset needed for *MESSENGER* data.

4 Total Electron Content: Methodology and measurement principle

The Total Electron Content (TEC) is defined as the total number of free electrons contained in a column (1 m^2 cross section) joining connecting the spacecraft and the receiver on Earth. It is calculated in the following way:

$$TEC = \int_{sat}^{rec} N_e(s)ds \qquad (9)$$

where N_e is the electron density calculated in e/m^3, while sat and rec indicates the position of the satellite and the Earth receiver respectively. The delay of a signal passing through the solar plasma depends on the electron density (Lopez Izurieta et al., 2022):

$$d_{plasma} = \int_{sat}^{rec} (n-1)ds \qquad (10)$$

Here, n is the refraction index and for the solar plasma it can be expressed as:

$$n = 1 - \frac{N_e e^2}{2\epsilon_0 m\omega^2} \qquad (11)$$

where e is the electron charge, m is the electron mass, ϵ_0 is the permittivity of free space and $\omega = 2\pi f$, where f is the carrier's frequency. Inserting Eq. (11) into Eq. (10), the delay becomes:

$$d_{plasma} = \frac{e^2}{2\epsilon_0 m\omega^2} TEC = \frac{e^2}{2\epsilon_0 m\omega^2} \int_{sat}^{rec} N_e(s)ds \qquad (12)$$

The delay due to the dispersive medium corresponds to the plasma signal obtained from

286 the calibrations of range observables. It's possible to retrieve the total electron content
287 by analysing the terms y_{pl_up} and y_{pl_dn} of Eq. (1), obtained during the radiotracking
288 passes. Ionospheric calibrations coming from GNSS (Global Navigation Satellite
289 System) data have been used (Runge 2008) to remove the Earth ionosphere contribution
290 from our dataset. Thus, the reported data show the contribution of interplanetary plasma
291 only.
292 Since the electron density model depends on the radial distance from the Sun, r (as
293 shown in Section 3), the integral along the line of sight from the definition of the TEC
294 (Eq. (9)) can be rewritten passing from ds to dr:

295 $$ds = \frac{rdr}{\sqrt{r^2 - b^2}}$$

296 $$r^2 = s^2 + b^2$$

297 where r is the radial distance and b the impact parameter.
298 Figure 4 reports the downlink TEC measured during two representative passes of SCE2,
299 on 8 and 12 February 2022. These two examples are used to illustrate two different
300 regimes of plasma content variability along the radio link: a strongly variable case and a
301 weakly variable case. The left panel corresponds to a central pass of the conjunction and

shows pronounced variability, likely associated with enhanced solar activity; the mean value is about 9570 TECU, with a standard deviation of about 1169 TECU, and maximum and minimum values of approximately 15075 and 8134 TECU, respectively. The right panel corresponds to a pass near the edge of the conjunction, where the TEC variability is much lower: the mean value is about 6505 TECU, with a standard deviation of about 142.7 TECU, and maximum and minimum values of approximately 7024 and 5964 TECU, respectively.

The delay induced by the solar plasma is proportional to the electron density, so the measurements from range observables can be used to improve density models. For each pass, the mean TEC value is fitted using a least-squares approach based on a theoretical electron density model (see section 3). To improve convergence towards the global minimum in the parameter space, a Particle Swarm Optimisation (PSO) algorithm (Kennedy and Eberhart, 1995; Eberhart and Kennedy, 1995) is first applied. The parameters obtained from the PSO are then used as the initial guess for the least-squares fit. The weights adopted in the least-squares procedure are calculated as the standard deviation of the residuals, i.e., the differences between the measured data and

318 the model predicted by the PSO solution.

319

320 **Figure 4** Downlink TEC measurements on 8 (left) and 12 (right) February 2022

321 (SCE2).

322

323 **5 Results**

324 First, we have analysed a two-terms model and, for our purposes, the Mercier-Hollweg

325 density profile was chosen, since it was observed to be the closest to the TEC data from

326 range observables with respect to the other two-terms profiles presented in Section 3;

327 moreover, we have also excluded models with three terms since the BepiColombo line

328 of sight didn't pass really close to the Sun's surface. The model of the electron density

329 to insert in the fitting procedure has the form:

330 $$N_e = \frac{a}{r^c} + \frac{d}{(r-1)^e} \quad e^-/m^3 \qquad (13)$$

331 where the parameters to be estimated are a, c, d and e, and r is the radial distance

332 from the Sun's centre expressed in solar radii. In the procedure the data from all five

333 conjunctions are taken into account, both on uplink and downlink. A PSO algorithm is

used to find the initial conditions for the least squares fitting. The density model which best fits the data is:

$$N_e = \frac{1.49 \cdot 10^{12}}{r^{2.58}} + \frac{1.03 \cdot 10^{11}}{(r-1)^{1.67}} \quad e^-/m^3 \qquad (14)$$

And the uncertainties on the parameters are reported in Table 1. However, it has been noticed that the estimated uncertainty on the coefficient d of the second term is high with respect to its central value ($\sigma_d = 4.27 \cdot 10^{11}$), meaning that the analysis is not sensitive to this term. The fitting procedure has been repeated including also data collected during cruise tests (with the line of sight at large impact parameters). The result is the following:

$$N_e = \frac{1.59 \cdot 10^{13}}{r^{4.49}} + \frac{2.75 \cdot 10^{11}}{(r-1)^{1.79}} \quad e^-/m^3 \qquad (15)$$

with the parameters' uncertainties reported in Table 1. The second term is similar to the previous result and they are compatible within 1σ. However, also in this case the coefficient of the second term presents a high uncertainty ($\sigma_d = 2.33 \cdot 10^{11}$).

Table 1 Uncertainties on the parameters of the two-terms model.

	Only SCE data	**SCE + end-to-end data**

$\boldsymbol{\sigma_a}$	$1.40 \cdot 10^{11}$	$1.01 \cdot 10^{9}$
$\boldsymbol{\sigma_c}$	$8.92 \cdot 10^{-1}$	$6.56 \cdot 10^{-1}$
$\boldsymbol{\sigma_d}$	$4.27 \cdot 10^{11}$	$2.33 \cdot 10^{11}$
$\boldsymbol{\sigma_e}$	$6.42 \cdot 10^{-1}$	$2.72 \cdot 10^{-1}$

Remarkably, these results suggest that the electron density at impact parameters higher than 4 solar radii can be expressed with a single radial term profile. Here, the method adopted by Bird et al. (1994) is considered. The model for the density is:

$$N_e = N_B \left(\frac{R_\odot}{r}\right)^{\alpha} e^{-}/m^3$$

where r is the distance from the Sun and $R_\odot$ is the solar radius. With this profile the TEC can be analytically integrated (Bird et al., 1994):

$$TEC(r) = K(\alpha) N_B R_\odot \left[\frac{R_\odot}{r}\right]^{\alpha-1} \qquad (16)$$

$$K(\alpha) = \int_{-\pi/2}^{\pi/2} \cos^{\alpha-2}\phi \, d\phi = \sqrt{\pi}\left[\frac{\Gamma\left(\frac{\alpha-1}{2}\right)}{\Gamma\left(\frac{\alpha}{2}\right)}\right]$$

Hence, the TEC data can be fitted using the expression in Eq. (16) and the parameters N_B and α can be estimated with the least squares procedure. The resulting density profile using SCE data is:

$$N_e = 1.325 \cdot 10^{12} \left(\frac{R_\odot}{r}\right)^{2.29} e^-/m^3 \qquad (17)$$

with uncertainties on the parameters reported in Table 2. The analysis has been repeated with the end-to-end data. The obtained model is:

$$N_e = 1.298 \cdot 10^{12} \left(\frac{R_\odot}{r}\right)^{2.28} e^-/m^3 \qquad (18)$$

and the uncertainties on the parameters are shown in Table 2. This result is compatible with the previous one considering the uncertainties within 1σ; thus, the model is valid both near the Sun and at large impact parameters.

Table 2 Uncertainties on the parameters of the single-term model.

	Only SCE data	**SCE + end-to-end data**
$\boldsymbol{\sigma_\alpha}$	0.104	0.094
$\boldsymbol{\sigma_{N_B}}$	$3.25 \cdot 10^{11}\ m^{-3}$	$2.90 \cdot 10^{11}\ m^{-3}$

Figure 5 represents the comparison between the TEC data and the TEC obtained from the two-terms and the single-term density models; the bottom plot is a zoom of the top plot showing the results for the impact parameters corresponding to the SCEs. The data

374 points are represented with the so called “candlesticks”: the thicker bar is centred in the
375 mean value of the TEC measured at each radiotracking pass and the height is given by
376 the standard deviation, while the thinner bar has the extremities corresponding to the
377 maximum and minimum value. The black curves indicate the results from the two-terms
378 model (dashed black line) and the single-term model (solid black line). It is possible to
379 observe that the two lines are almost superposed, meaning that the single-term density
380 model is well suitable to represent our data set without adding unnecessary complexity
381 in the model. The curves representing the original models analysed above are plotted as
382 a comparison: one can notice that the orange curve, corresponding to the Mercier-
383 Hollweg model, is the closest to our results and to the data. Instead, the other density
384 models differ significantly from the BepiColombo data: in fact, empirical models that
385 were retrieved using data from different missions with different solar conditions have
386 led to different results. Hence, analysing many data collected during different phases of
387 solar activity will help to improve our knowledge on the average behaviour of the
388 plasma electron density throughout the solar cycle.
389 From the density model it’s also possible to retrieve an expression for the refraction

index of solar plasma exploiting the relation in Eq. (11) and the resulting profile in Eq. (18):

$$n = 1 - \frac{N_e e^2}{2\epsilon_0 m\omega^2} = 1 - \frac{e^2}{2\epsilon_0 m\omega^2}\left[\frac{1.298 \cdot 10^{12}}{r^{2.28}}\right] \qquad (19)$$

where r is expressed in solar radii.

Figure 5 Comparison between the TEC data, the TEC obtained from the single-term density model (solid black line) and the TEC obtained from the best fit of Mercier-Hollweg profile (dashed black line) (top). The bottom figure represents a zoom near the Sun.

6 Conclusions

This work used BepiColombo multi-frequency range measurements acquired during five superior solar conjunction experiments to investigate empirical models of the coronal electron density. The calibrated plasma contribution to the range observables was converted into total electron content and used to test both two-terms and single-term radial density profiles, with particular focus on the Mercier-Hollweg model

406 (Wexler et al., 2019) and the single-power-law formulation of Bird et al. (1994). The
407 two-terms model was first fitted by estimating the coefficients and exponents of both
408 radial terms; however, the strong correlation between the two components, together
409 with the poor constraint on one of them, indicates that the additional term does not bring
410 a noticeable improvement in the fit. A single-term radial model was therefore favoured.
411 Notably, the analysis outlined that our data set is well-described by a single power law
412 function of the radial distance from the Sun's centre:

413 $$N_e = 1.298 \cdot 10^{12} \left(\frac{R_\odot}{r}\right)^{2.28} e^-/m^3$$

414 The analysis was repeated including cruise test data, acquired when the line of sight was
415 far from the Sun. Adding these points did not significantly change the model. Indeed,
416 the solutions with and without cruise data are compatible within 1σ. Finally, our
417 analysis shows that the applicability of any model is limited by the highly variable, non-
418 stationary solar activity (Figure 5). The favoured model can only be used to obtain an
419 average value of the solar plasma electron density as a function of the radial distance.
420 The TEC measurements indicate that the actual plasma density could be very distant
421 from the model when a CME or a solar flare occur.

In this work we have shown that multi-frequency range data can be used to study the electron density models of the plasma in the acceleration region of the solar wind, where a few in situ measurements from the Parker Solar Probe are available to date. The BepiColombo mission has provided a rich data set which lends statistical robustness to our results.

Declarations

Ethics approval and consent to participate

Not applicable

Consent for publication

Not applicable

Availability of data and materials

BepiColombo MORE data will be made available through the official ESA Planetary Science Archive (PSA), accessible at http://psa.esa.int (Besse et al., 2018). The calibrated plasma data used

in this study are presently available on Zenodo at https://doi.org/10.5281/zenodo.17813314 (Doria et al., 2025b), ensuring immediate accessibility.

Competing interests

The authors declare that they have no competing interests.

Funding

This work has been supported in part by the Italian Space Agency under agreement No. 2022-16-HH.1-2024

Authors' contributions

ID and PC defined the problem and the analysis methodology, ID performed the analysis, then they wrote the paper. LI is the PI of the MORE instrument: he provided the data and supervised the work.

Acknowledgements

Not applicable.

References

- Allen, C. W. (1947) Interpretation of Electron Densities from Corona Brightness. Monthly Notices of the Royal Astronomical Society, Volume 107, Issue 5-6, pp. 426–432
- Baumbach, S. (1937) Strahlung, Ergiebigkeit und Elektronendichte der Sonnenkorona. Astronomische Nachrichten, volume 263, Issue 6, p.121
- Benkhoff, J., Murakami, G., Baumjohann, W. et al. (2021) BepiColombo - Mission Overview and Science Goals. Space Sci Rev, 217, 90, https://doi.org/10.1007/s11214-021-00861-4
- Berman, A.L., and Wackley, J.A. (1977) Viking S-Band Doppler RMS Phase Fluctuations Used to Calibrate the Mean 1976 Equatorial Corona. DSN-PR, 42-38, p.152-166, Jet Propulsion Laboratory, Pasadena
- Bertotti, B., Comoretto, G., and Iess, L. (1993) Doppler Tracking of Spacecraft with Multi-frequency Links. Astron. Astrophys. 269, 608
- Besse, S., Vallat, C., Barthelemy, M., Coia, D., Costa, M., De Marchi, G., et al. (2018) ESA's Planetary Science Archive: Preserve and present reliable scientific

data sets. Planetary and Space Science, 150, 131–140, https://doi.org/10.1016/j.pss.2017.07.013

- Bird, M.K. (1982) Coronal Investigation with Occulted Spacecraft Signals. Space Sci Rev, 33, 99-126, https://doi.org/10.1007/BF00213250
- Bird, M.K., et al. (1994) The coronal electron density distribution determined from dual-frequency ranging measurements during the 1991 solar conjunction of the Ulysses spacecraft. The Astrophysical Journal, 426: 373-381
- Bird, M.K., et al. (1996) Coronal radio sounding with Ulysses: solar wind electron density near 0.1 AU during the 1995 conjunction. Astron. Astrophys., 316, pp. 441-448
- Cappuccio, P., Imamura, T., Doria, I., Chiba, S., di Stefano, I., Shiota, D., Asmar, S., Iess, L. (2024) Probing solar wind velocity from simultaneous superior solar conjunction radio science experiments of BepiColombo and Akatsuki missions. Monthly Notices of the Royal Astronomical Society, 533(2), pp 1560–1567, https://doi.org/10.1093/mnras/stae1929
- Doria, I., Cappuccio, P., Durante, D., di Stefano, I., Bernacchia, D., Lasagni

Manghi, R., et al. (2025a) Comparison of plasma calibration techniques to enhance radiometric observables performance: BepiColombo MORE test case. Radio Science, 60, e2025RS008441. https://doi.org/10.1029/2025RS008441

- Doria, I., Cappuccio, P., Durante, D., di Stefano, I., Bernacchia, D., Lasagni Manghi, R., et al. (2025b) BepiColombo calibrated plasma data [Dataset]. Zenodo. https://doi.org/10.5281/zenodo.17813314
- Eberhart, R., and Kennedy, J. (1995) A new optimizer using particle swarm theory. Proceedings of the 6th international symposium on micro machine and human science, pp 39–43, Nagoya, Japan, Mar 13–16, 1995
- Hollweg, J.V., et al. (2010) Coronal Faraday Rotation Fluctuations and a Wave/Turbulence Driven Model of the Solar Wind. The Astrophysical Journal, 722, pp. 1495-1503, doi: 10.1088/0004-637X/722/2/1495
- Iess, L., Asmar, S.W., Cappuccio, P., et al. (2021) Gravity, Geodesy and Fundamental Physics with BepiColombo's MORE Investigation. Space Sci Rev 217, 21, https://doi.org/10.1007/s11214-021-00800-3
- Johnston, D.W., Howe, T.W., and Rockwell, G.M. (1977) Viking mission

502 support. The Deep Space Network Progress Report 42, 38: 38-42

503 • Kennedy, J., Eberhart, R. (1995) Particle swarm optimization. Proc. IEEE
504 International Conf. on Neural Networks (Perth, Australia), IEEE Service Center,
505 Piscataway, NJ, 1995 (in press)

506 • Kliore, A. J., Anderson, J. D., Armstrong, J. W., Asmar, S. W., Hamilton, C. L.,
507 Rappaport, N. J., ... & Nagy, A. F. (2004) Cassini radio science. Space Science
508 Reviews, 115(1), 1-70, https://doi.org/10.1007/s11214-004-1436-y

509 • Lasagni Manghi, R., Bernacchia, D., Gomez Casajus, L., Zannoni, M., Tortora,
510 P., Martellucci, A., et al. (2023) Tropospheric delay calibration system
511 performance during the first two BepiColombo solar conjunctions. Radio
512 Science, 58, e2022RS007614, doi: 10.1029/2022RS007614

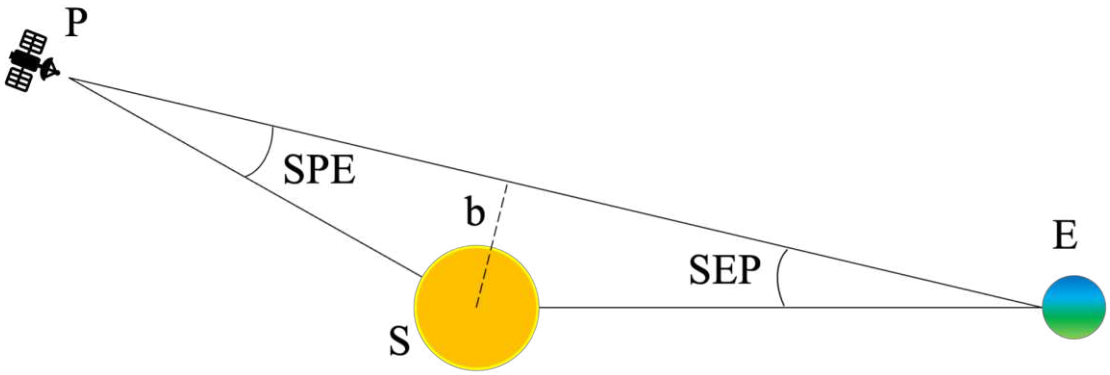
513 • Lopez Izurieta, E.D., Toapanta Guamanarca, E., and Barbier, H. (2022)
514 Ionospheric total electron content (TEC) above Ecuador. Journal of Physics,
515 Conf. Ser. 2238, 012010, doi:10.1088/1742-6596/2238/1/012010

516 • Mercier, C., and Chambe, G. (2015) Electron Density and Temperature in the
517 Solar Corona from Multifrequency Radio Imaging. Astronomy & Astrophysics,

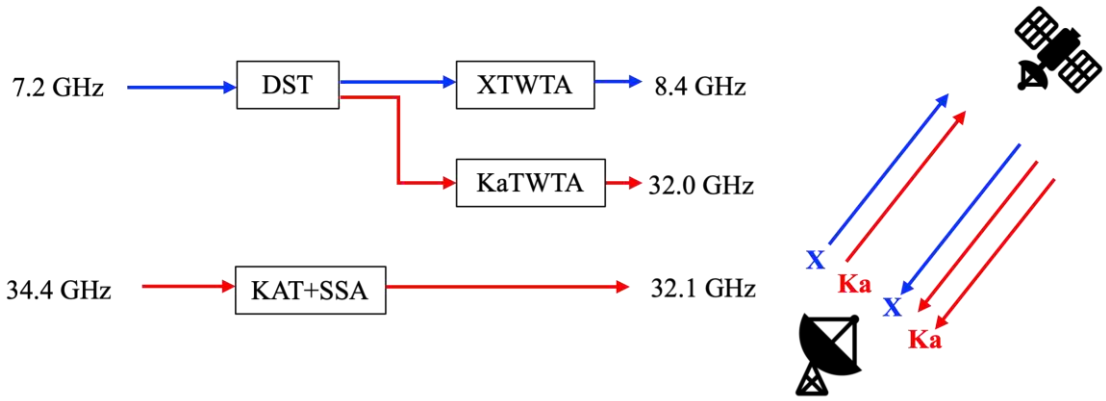
583 A101 (11pp), https://doi.org/10.1051/0004-6361/201425540

- Morabito, D.D. (2007) Solar corona-induced fluctuations on spacecraft signal amplitude observed during solar superior conjunctions of the Cassini spacecraft. Radio Science, 42(03), 1-16, doi: 10.1029/2005RS003425
- Muhleman, D.O., Esposito, P.B., and Anderson, J. D. (1977) The electron density profile of the outer corona and the interplanetary medium from Mariner-6 and Mariner-7 time-delay measurements. The Astrophysical Journal, 211:943-957
- Muhleman, D.O., and Anderson, J.D. (1981) Solar Wind Electron Densities from Viking Dual-Frequency Radio Measurements. The Astrophysical Journal, 247:1093-1101
- Runge, T. (2008) TRK-2-23 Media Calibration Interface. Deep Space Network (DSN) External Interface Specification, 820-013
- Soja, B., Heinkelmann, R., and Schuh, H. (2014) Probing the solar corona with very long baseline interferometry. Nature Communications, 5(1), 4166, https://doi.org/10.1038/ncomms5166

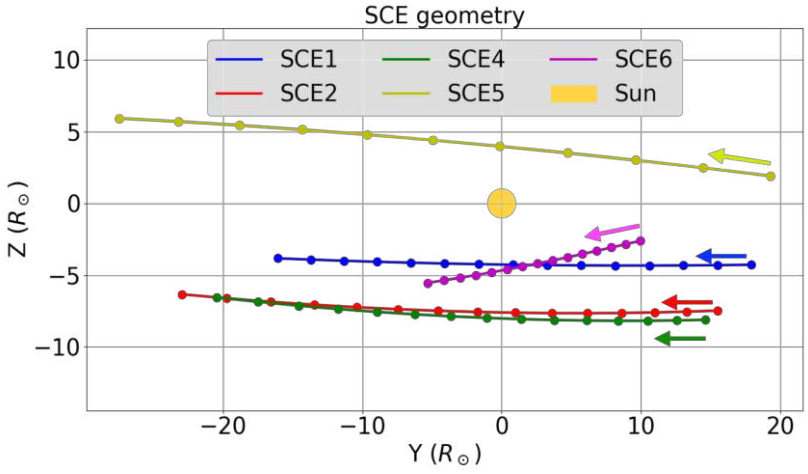
- Spangler, R.S., et al. (2002) Very Long Baseline Interferometer measurements of turbulence in the inner solar wind. Astronomy and Astrophysics, 384, 654-665, https://doi.org/10.1051/0004-6361:20020028
- Tortora P., L. Iess, et al. (2004) Precise Cassini Navigation During Solar Conjunctions Through Multifrequency Plasma Calibrations. Journal of Guidance, Control and Dynamics 27:2, 251-257, https://dx.doi.org/10.2514/1.997
- Tyler, G.L., et al. (1977) The Viking Solar Corona Experiment. Journal of Geophysical Research, 82, no. 28, https://doi.org/10.1029/JS082i028p04335
- Wexler, D.B., et al. (2019) Spacecraft Radio Frequency Fluctuations in the Solar Corona: A *MESSENGER-HELIOS* Composite Study. The Astrophysical Journal, 871:202 (13pp), doi: 10.3847/1538-4357/aaf6a8
- "Pseudo-noise (PN) ranging systems – Recommended standard CCSDS 414.1-B-3", Issue 3, Blue Book, Consultative Committee for Space Data Systems (CCSDS), NASA, Washington DC, USA, January 2022



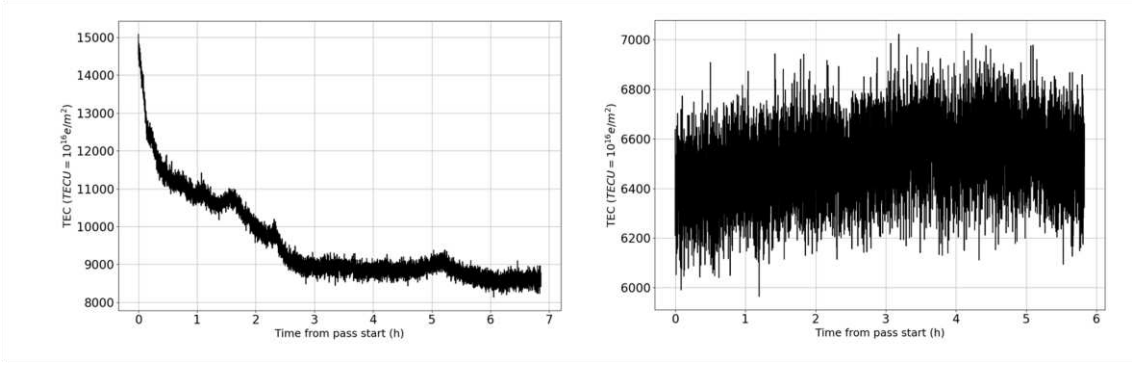
550



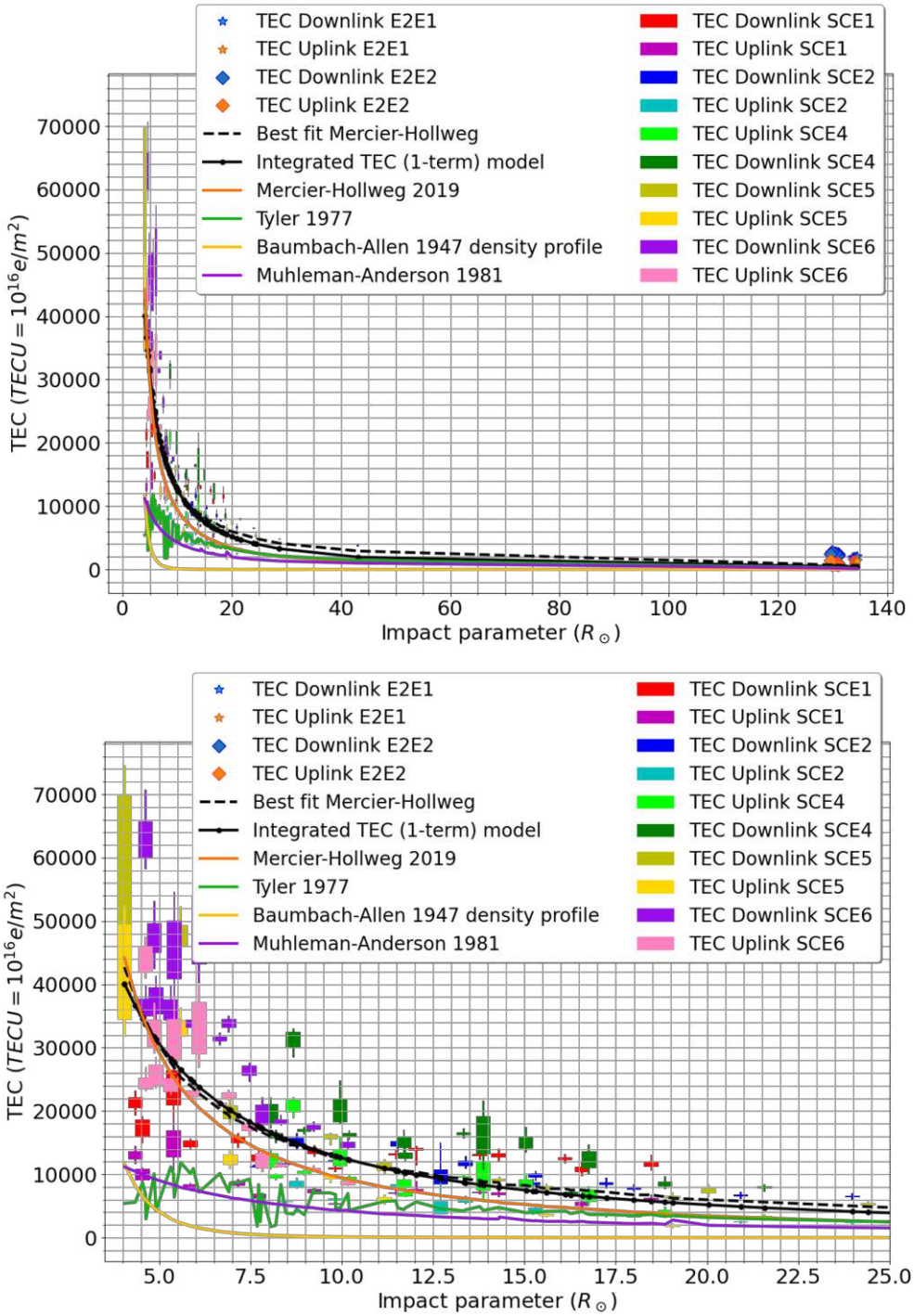
551



552



553


TEC Downlink E2E1
TEC Uplink E2E1
TEC Downlink E2E2
TEC Uplink E2E2
Best fit Mercier-Hollweg
Integrated TEC (1-term) model
Mercier-Hollweg 2019
Tyler 1977
Baumbach-Allen 1947 density profile
Muhleman-Anderson 1981
TEC Downlink SCE1
TEC Uplink SCE1
TEC Downlink SCE2
TEC Uplink SCE2
TEC Uplink SCE4
TEC Downlink SCE4
TEC Downlink SCE5
TEC Uplink SCE5
TEC Downlink SCE6
TEC Uplink SCE6
TEC (TECU = 10^16 e/m^2)
Impact parameter (R ⊙)

554

Supplementary Files

This is a list of supplementary files associated with this preprint. Click to download.

- Graphicalabstract.png